Title

Increasing Isoprene Epoxydiol-to-Inorganic Sulfate Aerosol Ratio Results in Extensive Conversion of Inorganic Sulfate to Organosulfur Forms: Implications for Aerosol Physicochemical Properties

Journal

Environmental Science and Technology, 53(15)

ISSN

0013-936X

Authors

Riva, Matthieu
Chen, Yuzhi
Zhang, Yue
et al.

Publication Date

2019-08-06

DOI

10.1021/acs.est.9b01019

Peer reviewed

Published in final edited form as:

Environ Sci Technol. 2019 August 06; 53(15): 8682–8694. doi:10.1021/acs.est.9b01019.

Increasing Isoprene Epoxydiol-to-Inorganic Sulfate Aerosol (IEPOX:$Sulf_{inorg}$) Ratio Results in Extensive Conversion of Inorganic Sulfate to Organosulfur Forms: Implications for Aerosol Physicochemical Properties

Matthieu Riva[†,#,¥,*], **Yuzhi Chen**[†,¥], **Yue Zhang**[†,§], **Ziying Lei**[‖], **Nicole E. Olson**[⊥], **Hallie C. Boyer**[#], **Shweta Narayan**[#], **Lindsay D. Yee**[▽], **Hilary S. Green**[†,‡], **Tianqu Cui**[†], **Zhenfa Zhang**[†], **Karsten Baumann**[○], **Mike Fort**[○], **Eric Edgerton**[○], **Sri H. Budisulistiorini**[†,♦], **Caitlin A. Rose**[†], **Igor O. Ribeiro**[¶], **Rafael L. e Oliveira**[¶], **Erickson O. dos Santos**[∞], **Cristine M. D. Machado**[∞], **Sophie Szopa**[∏], **Yue Zhao**[¬,"], **Eliane G. Alves**[$], **Suzane S. de Sá**[□], **Weiwei Hu**[•], **Eladio M. Knipping**[~], **Stephanie L. Shaw**[¨], **Sergio Duvoisin Junior**[¶], **Rodrigo A. F. de Souza**[¶], **Brett B. Palm**[•], **Jose-Luis Jimenez**[•], **Marianne Glasius**[¨], **Allen H. Goldstein**[▽], **Havala O. T. Pye**[†,þ], **Avram Gold**[†], **Barbara J. Turpin**[†], **William Vizuete**[†], **Scot T. Martin**[□,»], **Joel A. Thornton**[¬], **Cari S. Dutcher**[#], **Andrew P. Ault**[‖,⊥,*], **Jason D. Surratt**[†,*]

[†]Department of Environmental Sciences and Engineering, Gillings School of Global Public Health, The University of North Carolina at Chapel Hill, Chapel Hill, NC 27599, USA

[§]Aerodyne Research Inc., Billerica, MA 01821, USA

[‖]Department of Environmental Health Sciences, University of Michigan, Ann Arbor, MI 48109, USA

[⊥]Department of Chemistry, University of Michigan, Ann Arbor, MI 48109, USA

[#]Department of Mechanical Engineering, University of Minnesota-Twin Cities, Minneapolis, MN 55455, USA

[▽]Department of Environmental Science, Policy, and Management, University of California, Berkeley, CA 94720, USA

[*]**Corresponding Author** (M. R.): matthieu.riva@ircelyon.univ-lyon1.fr, (A. P. A.): aulta@umich.edu, (J. D. S.): surratt@unc.edu.
[¥]These authors contributed equally to this work
[#]Now at the Univ Lyon, Université Claude Bernard Lyon 1, CNRS, IRCELYON, F-69626, Villeurbanne, France.
[‡]Now at Department of Food Science and Technology, University of California, Davis, Davis, CA 95616, USA.
[♦]Now at Earth Observatory of Singapore, Nanyang Technological University, Singapore 639798, Singapore.
["]Now at School of Environmental Science and Engineering, Shanghai Jiao Tong University, Shanghai, 200240, China.

ASSOCIATED CONTENT

The materials and methods provide additional information on the collection of $PM_{2.5}$ performed during the different field campaigns. In addition, more details on the chemical characterization of the organosulfur compounds are also proposed. Finally, the thermodynamic model of aerosol pH is explained. Figures S1 and S2 show the representative Taylor plots and the interfacial tensions of the main IEPOX-derived SOA components, respectively. Figures S3–S5 show the mass concentrations of aerosol sulfate and organosulfur compounds as well as their contribution to the mass of sulfate. Figure S6 compares the modelled aerosol pH when considering vs not considering IEPOX-OS. Figure S7 shows AFM amplitude and phase images, and SEM images of IEPOX-OA. Figure S8 shows the diel-profiles of the RH in the amazon forest during the wet and dry season as well as the concentration of isoprene. Figure S9 presents the interfacial tension of 2-MT. Figure S10 shows the gas-phase concentration of IEPOX during chamber experiments. The tables provide a summary of experimental conditions as well as a summary of the different organosulfates identified in SOA collected during the different field campaigns. This material is available free of charge via the Internet at http://pubs.acs.org/.

○Atmospheric Research & Analysis, Inc., Cary, NC 27513, USA

¶Escola Superior de Tecnologia, Universidade do Estado do Amazonas, Manaus, Amazonas, 69050, Brasil

∞Department of Chemistry, Federal University of Amazonas, Manaus, Amazonas, 69067, Brazil

∏Laboratoire des Sciences du Climat et de l'Environnement, CEA-CNRS-UVSQ-IPSL, 91190, Gif-sur-Yvette, France

¬Department of Atmospheric Sciences, University of Washington, Seattle, WA 98195, USA

$Environment Dynamics Department, National Institute of Amazonian Research (INPA), Manaus, 69067, Brazil

□John A. Paulson School of Engineering and Applied Sciences, Harvard University, Cambridge, MA 02138, USA

•Department of Chemistry and Cooperative Institute for Research in Environmental Sciences, University of Colorado, Boulder, CO 80309, USA

~Electric Power Research Institute, Washington, D.C 20005, USA

⋯Electric Power Research Institute, Palo Alto, CA 94304, USA

¨Aarhus University, Dept. of Chemistry, 8000 Aarhus C, Denmark

þNational Exposure Research Laboratory, US Environmental Protection Agency, Research Triangle Park, NC 27711, USA

»Department of Earth and Planetary Sciences, Harvard University, Cambridge, MA 02138, USA

Abstract

Acid-driven multiphase chemistry of isoprene epoxydiols (IEPOX), key isoprene oxidation products, with inorganic sulfate aerosol yields substantial amounts of secondary organic aerosol (SOA) through the formation of organosulfur compounds. The extent and implications of inorganic-to-organic sulfate conversion, however, are unknown. In this report, we demonstrate that extensive consumption of inorganic sulfate occurs, which increases with the IEPOX-to-inorganic sulfate concentration ratio (IEPOX:$Sulf_{inorg}$), as determined by laboratory measurements. Characterization of total sulfur aerosol observed at Look Rock, Tennessee, from 2007–2016 shows that organosulfur mass fractions will likely continue to increase with ongoing declines in anthropogenic $Sulf_{inorg}$, consistent with our laboratory findings. We further demonstrate that organosulfur compounds greatly modifies critical aerosol properties, such as acidity, morphology, viscosity, and phase state. These new mechanistic insights demonstrate that changes in SO_2 emissions, especially in isoprene-dominated environments, will significantly alter biogenic SOA physicochemical properties. Consequently, IEPOX:$Sulf_{inorg}$ will play an important role in understanding historical climate and determining future impacts of biogenic SOA on global climate and air quality.

Graphical Abstract

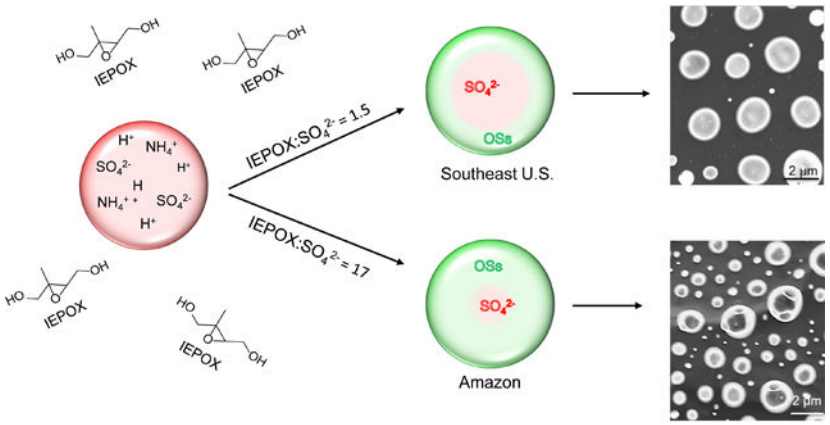

Keywords

SOA; mass spectrometry; heterogeneous chemistry; reactive uptake

Introduction

Secondary organic aerosol (SOA) formed through the oxidation of volatile organic compounds is a major and globally ubiquitous component of atmospheric fine particulate matter ($PM_{2.5}$; aerosol particles ≤ 2.5 μm in aerodynamic diameter).[1] Chemical composition of fine particles determines aerosol physicochemical properties, such as viscosity and phase state, and plays a central role in the effects of SOA on air quality and climate.[2,3] Understanding how SOA forms and interacts with other gas- and particle-phase species is crucial to accurately evaluating its importance in the Earth's climate system and adverse effects on public health.

Inorganic sulfate species (e.g., SO_4^{2-}, HSO_4^-) are also a significant $PM_{2.5}$ component with the capacity to impact atmospheric composition and climate, in part, because of its predicted impact on aerosol acidity, hygroscopicity, visibility and cloud nucleation.[1,4] The oxidation of sulfur dioxide (SO_2) to sulfuric acid (H_2SO_4) increases aerosol acidity, which enhances SOA formation.[4–8] Sulfur in the form S(VI) in aerosols was generally assumed to be primarily present as inorganic sulfate (SO_4^{2-} and HSO_4^-) ions until more recent studies revealed the presence of organosulfur components in $PM_{2.5}$.[9–13] Despite observations that organosulfur compounds are important contributors to SOA mass in a range of environments globally,[14–20] estimations of aerosol acidity and liquid water content typically assume that only inorganic sulfate plays a role.[21] Correctly identifying the chemical form of sulfur (i.e., inorganic vs. organic), and representing it accurately in atmospheric models is essential as the different forms lead to different aerosol physicochemical properties that will have different predicted impacts on air quality and climate.[3]

Laboratory studies have demonstrated that acid-driven multiphase chemistry (reactive uptake) of isoprene epoxydiols (IEPOX) is key to explaining the chemical form and extent of SOA formation from photochemical oxidation of isoprene [22–25] and field measurements have confirmed this is the predominant pathway.[26–31] While chamber studies have shown

that organosulfur compounds, specifically organosulfates (OS) [32] formed by the reactive uptake of IEPOX with particulate inorganic sulfate ($Sulf_{inorg}$), contribute significantly to IEPOX-SOA,[33,34] the extent and implications of sulfate conversion to organic forms have remained unknown.

Combined laboratory, field, and modeling studies described in this study reveal the hitherto unrecognized effect that acid-driven multiphase chemistry of IEPOX may result in substantial conversion of $Sulf_{inorg}$ to organosulfur compounds. Laboratory experiments reveal that the extent of $Sulf_{inorg}$ conversion is greater for high IEPOX:$Sulf_{inorg}$ ratios (such as observed in the Amazon) than for lower ratios (such as observed in the Southeastern United States (SE U.S.)). Assuming IEPOX concentration remains constant, continuing $Sulf_{inorg}$ reductions in the Northern Hemisphere as a consequence of SO_2 emission controls are thus expected to greatly increase the fraction of $Sulf_{inorg}$ converted in the future. High IEPOX:$Sulf_{inorg}$ scenario also likely characterized pre-industrial atmospheric conditions. Changes in the ratio over time and the consequent changes in SOA chemical composition and physicochemical properties will increase understanding of the evolution of climate change and inform projections for the future.

Experimental Methods

Smog Chamber Experiments.

Experiments were performed in the indoor environmental chamber facility at the University of North Carolina. The experimental setup and analytical techniques used in this work have been described in detail elsewhere [33,35]. Briefly, experiments were carried out under dark and wet conditions (50 ± 4 %, relative humidity (RH)) at 296 ± 1 K in a 10-m^3 Teflon chamber. A summary of the experimental conditions is provided in Table S1. Prior to each experiment, the chamber was flushed continuously with clean air for ~ 24 hours corresponding to a minimum of seven chamber volumes until the particle mass concentration was < 0.01 μg m^{-3}. Chamber flushing also reduced VOC concentrations below the detection limit (i.e., ~ 75 ppt for IEPOX). Temperature and RH in the chamber were continuously monitored using a dew point meter (Omega Engineering Inc.). Acidified ammonium sulfate seed aerosols were injected into the pre-humidified chamber using a custom-built atomizer with an aqueous solution of 0.06 M $(NH_4)_2SO_4$ (aq) and 0.06 M H_2SO_4 (aq) until the desired total aerosol mass concentration was achieved. After seed injection, the chamber was left static for at least 30 min to ensure that the seed aerosol stability and uniform mixing. The IEPOX vapor was generated by using a high-purity N_2 (g) flow of 2 L min^{-1} for 10 min and then 4 L min^{-1} for 50 min through a heated manifold (60°C) containing a known amount of pure *trans-β*-IEPOX (synthesized in house[36]) dissolved in ethyl acetate. This approach to introduce IEPOX has been used in previous studies.[33, 37, 38]

Aerosol size distributions were continuously measured using a differential mobility analyzer (DMA, BMI model 2002) coupled to a mixing condensation particle counter (MCPC, BMI model 1710) in order to monitor aerosol number, surface area, and volume concentration within the chamber. SOA generated from the reactive uptake of IEPOX was collected using a particle-into-liquid sampler (PILS, BMI model 4001) throughout each experiment. PILS

samples were collected at 5 min intervals for offline chemical analysis by ion chromatography (IC) and ultra-performance liquid chromatography interfaced to electrospray ionization high-resolution quadrupole time-of-flight mass spectrometry (UPLC/ESI-HR-Q-TOFMS). The PILS vials were stored in the dark at 2°C immediately after collection and analyzed within 24 h without further pretreatment. PILS operating conditions and dilution correction are described in the SI.

Flow Tube Experiments.

The reactive uptake coefficient of IEPOX (γ_{IEPOX}) is an important model-relevant parameter that characterizes the heterogenous chemistry of IEPOX.[24, 36] Direct measurement of γ_{IEPOX} onto aqueous ammonium bisulfate (ABS) particles was conducted at the University of Washington in an aerosol flow tube coupled to an iodide-adduct chemical ionization mass spectrometry (CIMS); operating conditions have been described elsewhere and in the SI.[37,38]

Collection of $PM_{2.5}$ samples.

Ambient SOA ($PM_{2.5}$) samples from two isoprene-dominated environments (SE-U.S. and Amazon forest) were collected onto quartz filters during three field campaigns: (i) during the 2013 Southern Oxidant and Aerosol Study (SOAS) campaign from 1 June to 15 July 2013 at the Centerville, AL (CTR, AL) ground site; (ii) from 18 July through 1 August 2016 from downtown Manaus, Brazil and (iii) during the Green Ocean Amazon (GoAmazon2014/5) field campaign[39] during intensive operating period 2 (IOP2). Additional information regarding filter collection is provided in SI.

Aerosol Chemical Characterization.

Chemical characterization of $PM_{2.5}$ and PILS samples was performed by UPLC/ESI-HR-Q-TOFMS (6520 Series, Agilent) operated in the negative ion mode.[40,41] Total water-soluble organosulfur compound mass was determined from the difference between total water-soluble sulfur measured by isotope ratio inductively coupled plasma mass spectrometry (IR-ICP-MS) and sulfate-sulfur (sulfur in the form of inorganic sulfate/$Sulf_{inorg}$) measured by IC on the same sample aliquot. Sample extractions, operating conditions, standard preparation, and uncertainty estimates are described in detail in SI. The National Park Service Improve database[42] was used to evaluate the inorganic sulfate and organosulfur mass concentrations in the SE-U.S from 2007 to 2016.

Microscopy Imaging.

Morphology of aerosol particles collected before, during, and after IEPOX reactive uptake from smog chamber experiments was characterized by atomic force microscopy (AFM) and scanning electron microscopy (SEM). Additional information regarding operating conditions is provided in SI and prior publications.[43–45]

Biphasic Microfluidics.

Surface and interfacial tensions inform solute surface-bulk partitioning and, therefore, the availability of compounds for interactions with the ambient gaseous phase, such as

heterogenous chemistry and water uptake. Lower interfacial tensions due to organic partitioning affect both particle growth and structure. We measured liquid-liquid interfacial tensions of IEPOX SOA tracer 2-methyltetrols (2-MT) and its OS derivative (3-methyltetrol sulfate, IEPOX-OS) using a biphasic microfluidic platform. Droplet microfluidics as a method to measure interfacial tension for aerosol science applications was first introduced for studying the aging of SOA aerosols,[46] using a microtensiometry technique described in detail in several studies and in the SI.[47–51] The microfluidic chip is fabricated using standard soft-lithography techniques [52–54] and mounted on an inverted microscope. Two immiscible liquid phases separately enter the device by pressure-driven flow, [51] and droplet breakup is induced by a flow-focusing geometry [55–57] Aqueous solutions containing the SOA are the dispersed (droplet) phase, and silicone oil is the carrier (continuous) phase. The droplets of aqueous SOA then enter a contraction geometry in the microfluidic channel, which induces deformation of the liquid-liquid interface. This deformation, is imaged at high speed, and related to material and flow-field properties [48,49,58–61] to calculate the interfacial tension between silicone oil and aqueous SOA solutions. The equation governing droplet deformation is:

$$\alpha\eta_c\left(\frac{5}{2\hat{\eta}+3}\dot{\varepsilon}(x)-u(x)\frac{\partial D(x)}{\partial x}\right)=\sigma\frac{D(x)}{a_0}. \quad (1)$$

In the above equation, α is a function of the viscosity ratio $\hat{\eta}$, which is a ratio of the dispersed phase viscosity (here, the aqueous phase viscosity is close to that of pure water – 1 mPa s – near 100% RH for aerosol droplets), to the continuous phase viscosity η_c (here, the viscosity of silicone oil – 50 mPa s). For solutions containing 1.55 M ammonium sulfate (AS), the viscosity is 1.215 mPa s.[62] $\dot{\varepsilon}(x)$ is the extensional strain rate in the contraction, $u(x)$ is the velocity of the droplet centroid, $D(x)$ is the deformation, a_0 is the un-deformed diameter of the spherical droplet, and σ is the interfacial tension between the aqueous and oil phase. $D(x)$ is defined by Taylor [58–60] as $D(x)=\frac{d_{major}-d_{minor}}{d_{major}+d_{minor}}$, where d_{major} and d_{minor} are the major and minor diameters of the deformed droplet respectively, measured using image analysis. A plot of the left side of the equation of motion versus $\frac{D(x)}{a_0}$ is linear in the small-deformation regime [58,60]. A straight line is fit to the linear portion of the curve, known as a "Taylor plot", and the slope of the line is equal to the interfacial tension.

Each microfluidic measurement consumes 250–300 μL of aqueous solution, yielding 20–30 droplets. The IEPOX-OS droplet interfacial tensions reported in this work were statistically averaged. All interfacial tension values reported in this work are then normalized by the interfacial tension of pure water with silicone oil measured with microfluidics (30 mN/m). Figures S1 and S2 show Taylor plots and interfacial tensions for 2-MT and IEPOX-OS samples. The surface partitioning of SOA is analogous to that expected to occur in aerosol droplets in the atmosphere, as discussed in Metcalf et al.[51] Techniques for measurement of interfacial tension using biphasic microfluidics are outlined in prior work.[51,63]

Viscosity Model.

The viscosity of IEPOX-derived OS is calculated based on a modified version of the Vogel-Tammann-Fulcher (VTF) equation (Eqs. 2 & 3) by Angell et al.[64,65]

$$\eta(RH) = \eta_{\infty} e^{\frac{T_0 D}{T - T_0}} \quad (2)$$

where η_{∞} is viscosity at infinite temperature and assumed to be 10^{-5} Pa s; T_0 is the Vogel temperature; T is the ambient temperature; and D is the fagility parameter, which controls how closely a material follows the Arrhenius law.[64] When T reaches glass transition temperature T_g, η reaches 10^{12} Pa s. Then Eq. 2 becomes

$$T_g / T_0 = 1 + 0.0255D \quad (3)$$

Both D and T_g are required to calculate η for SOA-water mixtures at a given temperature. The T_g of each SOA compound comprising the SOA under dry conditions was estimated based on the improved paramterizaiton described in DeRieux et al.[66] Then Gordan-Taylor mix rule (Eq. 8 in the SI) was applied to calculate the T_g of SOA mixtures. A detailed description of the workflow and choices of parameters used in calculating the viscosity of IEPOX-derived OS is given in the SI.

Thermodynamic Model of Aerosol pH.

The pH of aerosol particles during the heterogenous reaction processes of IEPOX is calculated with smog chamber data using a thermodynamic model employing two methods. Briefly, the first method uses measured $Sulf_{inorg}$ concentration as well as the NH_4^+ concentration at the beginning of the experiment as the input variables. The concentrations of IEPOX-OS and oligomeric OS are not considered. While retaining the inorganic cations and anions considered in the first scenario, the second method takes the anions of IEPOX-OS monomer as well as its dimers and trimers into consideration. The proton balance equation together with the mass balance equations for NH_4^+, SO_4^{2-}, HSO_4^-, and IEPOX-OS monomers, dimers, and trimers were built to solve the H^+ ion concentration. The gas-particle equilibrium of NH_3 and NH_4^+ was considered using a Henry's law constant of 0.0161 atm M^{-1}. A growth factor of 1.3 was used to calculate the liquid water content of the particles. Similar to the ISORROPIA-II model,[67] the activity coefficients for all ions were assumed to be 1 in this case. The uncertainties in the growth factor of the particle, the activity coefficient of each ion, and the pKa values of organosulfur species contribute to the overall uncertainty of this model. These factors may affect the exact values of the pH calculated; however, the drastic difference of the pH values between considering and not considering the organosulfur species remains roughly the same. A detailed description of the thermodynamic model is given in the SI.

Global Modeling.

The IEPOX:$Sulf_{inorg}$ mass ratio has been computed based on numerical simulations performed with the LMDz-OR-INCA global climate-chemistry model. The description of

the model representation for sulfate as well as the general features of the LMDz-OR-INCA model can be found in Szopa et al. [68] The reaction mechanism of IEPOX is based on St Clair et al.[69] and considers three different isomers of IEPOX produced by three different geometrical configurations of the isoprene hydroxyperoxide (ISOPOOH) precursor produced through the isoprene oxidation.

The LMDz-OR-INCA model is used with a 3.8° lat × 1.87° lon horizontal resolution and 39 vertical levels. The wind fields are nudged on the ECMWF (European Centre for Medium-Range Weather Forecasts) reanalysis for the year of 2010 (considering first a one-year spin-up). The anthropogenic emissions are those from the Representative Concentration Pathways (RCP) considering the year 2010 in the 8.5 trajectory (compatible with the evolution of radiative forcing equivalent in 2100 to 8.5 $W.m^{-2}$)[70]. The biomass burning emissions correspond to the GFED-v4 inventory for the year of 2010. The anthropogenic, ship and fire emissions of SO_2 are respectively 40.5, 5.9 and 1.1 TgS yr^{-1}. The biogenic emissions are computed by the ORCHIDEE vegetation model as described elsewhere [71]. They lead to a global annual isoprene emission of 466 TgC yr^{-1} inducing a production of IEPOX of 115 TgC yr^{-1}, which is consistent with the one found by St Clair et al. [69]

Results and Discussion

IEPOX conversion of $Sulf_{inorg}$ to organosulfur.

Despite the wealth of studies on the reactive uptake of IEPOX, its reactivity remains poorly constrained.[24,25,28,33,40,72] We performed controlled chamber experiments in the presence of ABS seed particles (pH = 1.5) at ~50 % RH using atmospherically-relevant ratios of IEPOX:$Sulf_{inorg}$ (SI Table S1). Figure 1 shows that immediately following IEPOX addition, rapid conversion of $Sulf_{inorg}$ is observed under all conditions measured by the PILS coupled to an IC system operated with 5-minute resolution. The rate of $Sulf_{inorg}$ depletion correlates with the formation of IEPOX-OS and oligomeric-OS (quantified by UPLC/ESI-HR-Q-TOFMS for the same PILS samples), which is further supported by computational chemistry modeling by Piletic et al. that suggests IEPOX would readily produce OSs in acidic aerosols. [73] IEPOX-OS accounts for most (90–100%) of the $Sulf_{inorg}$ converted within the first 40–60 min under conditions that mimic IEPOX:$Sulf_{inorg}$ ratios relevant to both the SE-U.S. (Figure 1A) and the Amazon (Figure 1B). As shown in Figures 1A and B, ~40% of $Sulf_{inorg}$ injected into the chamber is converted to organosulfur under laboratory conditions that mimic the SE-U.S. conditions, while up to 90% is converted to organosulfur under laboratory conditions that mimic the Amazon. During the next hour following the termination of IEPOX injection, $Sulf_{inorg}$ as well as total organic sulfate has stabilized, indicating inhibition of IEPOX uptake (discussed below), then a decrease of concentrations of IEPOX-OS commences. A net reduction (up to 30% in one hour) of the three quantified OS species indicates that IEPOX-OS are not stable and react to yield as yet uncharacterized organosulfur compounds. One potential class of species, sulfur-containing oligomers, were observed below quantifiable levels in the positive ion mode.

Our results demonstrate the conversion of inorganic-to-organic sulfate is driven primarily by the IEPOX:$Sulf_{inorg}$ ratio as illustrated in Figure 1C. From our laboratory experiments, the IEPOX:$Sulf_{inorg}$ ratio appears to be a critical, previously unrecognized factor in the

conversion of inorganic-to-organic sulfate. By extrapolating our laboratory findings to ambient conditions, high IEPOX:$Sulf_{inorg}$ ratios (>2) are common globally, as shown in Figure 1D, especially in equatorial regions and the Southern Hemisphere, and might be important in the formation of organic sulfate 9in such areas. Based on our experimental results, we infer that a higher S(VI) fraction is likely in organic forms in those regions, which are under-sampled relative to the Northern Hemisphere.

Concentration of ambient organosulfur compounds.

Over the past 30 years, air pollution regulations in the Northern Hemisphere have led to decreases in SO_2 concentration of 5.7 % yr^{-1} in the U.S. and 5.1 % yr^{-1} in Europe.[74] Recent studies project a reduction of SO_4^{2-} of ~4.5% yr^{-1} based on current efforts.[75,76] Figure 2A illustrates this trend and presents the SO_4^{2-} concentration over the last 10 years measured at the Great Smoky Mountain Site (Look Rock, TN) through the IMPROVE monitoring program,[42] which is strongly influenced by isoprene chemistry.[27] A decrease of $Sulf_{inorg}$ by a factor of 6 is correlated with a subsequent rise in organosulfur as a fraction of total sulfur by a factor of 5. In addition, events with high organosulfur fractions tend to correlate with low $Sulf_{inorg}$ concentrations (Figure 2B), consistent with a previous analysis[12] and corroborating our laboratory findings. Assuming a constant IEPOX concentration and a reduction of SO_4^{2-} of ~4.5% yr^{-1}, the increase in the IEPOX:$Sulf_{inorg}$ ratios within the next decades is expected to significantly shift the distribution of S(VI) towards organosulfur (Figure 1C). Since industrialization, $Sulf_{inorg}$ has significantly increased[77,78] while the concentration of isoprene has remained constant.[79] This trend indicates that IEPOX:$Sulf_{inorg}$ was likely much higher during the pre-industrial period than currently, and possibly had a major role in SOA physicochemical properties in isoprene-dominated areas. While the estimated conversion extrapolated from our chamber experiments is likely an upper limit as the reactive uptake of IEPOX is sensitive to aerosol acidity and other factors in the ambient environments (e.g. NO_x, organic coating, RH, etc.), the trend identified in this study is central to understanding future air quality and radiative forcing.

Molecular characterization of SOA samples collected in isoprene-rich areas show that OS alone contribute a substantial mass fraction of S(VI) in PM: from 8 to 25% in the SE-U.S. and from 20 to 45% in downwind Manaus (Figure 2C and SI Figure S1). From direct comparison between ICP-MS and AMS sulfate data (Figure S3), we applied a correction factor (i.e., 1.28) in order to account for the subset of organosulfur compounds present within the size range of 1 to 2.5 microns. OS mass ranges from 400–1500 ng m^{-3}, at the high end of previous studies (SI Tables S2–S4).[26,27,32,80,81] While the sum of OS in the SE-U.S. is significantly different from that of downwind Manaus, isoprene-OS nevertheless represents the predominant OS in both areas. During the 2013 SOAS campaign, total mass concentrations of organosulfur compounds were also determined by IR-ICP-MS (SI Figure S4). The average total sulfur mass multiplied by three (3 × S) and the total $Sulf_{inorg}$ measured by IR-ICP-MS and IC, respectively, differs by 300 ± 200 ngSO_4 m^{-3}. The difference represents an estimate of total organosulfur compounds and provides an organosulfur/total sulfur ratio similar to that previously observed.[12,13,82] Although total OS + MSA exhibits a strong correlation (r^2 = 0.78) with the total mass concentration of organosulfur compounds (SI Figure S5), the identified products explain only 50–60% of the

total mass of organosulfur quantified in $PM_{2.5}$ during the 2013 SOAS field campaign. Assuming similar C:S ratios for identified and unidentified compounds, 16% of the $Sulf_{inorg}$ is converted into organosulfur compounds (SI Figure S5). In fact, using the fit obtained from all chamber experiments (Figure 1C) and an IEPOX:$Sulf_{inorg}$ ratio of 0.24 estimated based on collocated measurements during the 2013 SOAS campaign,[83] $Sulf_{inorg}$ conversion to organosulfur is estimated to be ~15%. This is in excellent agreement with the characterizations of field SOA samples presented above.

Atmospheric impact of the acid-driven reactive uptake of IEPOX.

In the following section, we show significant alterations of aerosol physicochemical properties due to high levels of inorganic-to-organic sulfate conversion in the chamber experiments. Explored properties include aerosol acidity, morphology, surface tension, viscosity, and reactivity.

Because acidity is one of the governing factors of atmospheric multiphase chemistry,[6] the response of condensed-phase acidity to inorganic-to-organic sulfate conversion was further investigated. The widely used thermodynamic models treat sulfate as inorganic S(VI), leading to inconsistencies in charge balance in the condensed phase.[84,85] While organic compounds can reduce the rate of ammonia gas-to-particle partitioning, exclusion of organosulfur compounds such as OSs from thermodynamic models may outweigh this effect and contribute to an even larger discrepancy in acidity. Hence a thermodynamic model was constructed to estimate the acidity of the aerosols from these experiments with and without organosulfur compounds. The model assumes all the components reach thermodynamic equilibrium with the hydrogen ion, while maintaining charge balance and mass balance, similar to previous publications.[67,86,87] The detailed parameterization of the thermodynamic model is described in the SI. As an example, Figure S6 shows the pH of aerosols when not considering the contributions of IEPOX-OS to acidity from the chamber experiments, compared to a thermodynamic box model constructed to take IEPOX-OS into consideration. Aerosol compositions measured at the end of the chamber experiments were used as input to calculate aerosol pH as shown in Figure S6. If the contributions of IEPOX-OS to acidity were not considered, the aerosol pH would have been overestimated by 3.5 and 9.5 units in the laboratory mimic of SE U.S. and Amazon, respectively. The pK_a values of IEPOX-OS remain uncertain. By varying the pK_a values of IEPOX-OS in the range of 0–4, the aerosol acidity changes up to 6 times (0.8 pH units), suggesting the importance of further research on determining the pK_a values of IEPOX-OS and their roles in governing the aerosol acidity.

Acid-driven multiphase chemistry of IEPOX also leads to a modification of the aerosol morphology from a well-mixed sphere to a core-shell structure, shown by height images obtained by AFM at ambient temperature and pressure (Figures 3A–C), as well as AFM amplitude images, AFM phase images and SEM images (Figure S7) of SOA collected from the chamber experiments. It is noted that the AFM images of the laboratory-derived SOA were collected at ambient pressure and RHs close to chamber conditions (30–40%). SEM data were collected after equilibration under vacuum (10^{-3} to 10^{-5} Pa). RH was not cycled for these specific particles to check morphology, but has been either cycled or tested at multiple RH values in a recent study.[88] This study demonstrated that the core-shell structure

was not substantially altered by the RH cycling beyond efflorescence and deliquescence of the ammonium sulfate core. Additionally, SEM and AFM images were collected under different conditions, but showed similar morphology, supporting the hypothesis that for the more viscous particles in this study, temperature and RH differences during imaging had minimal effect on the particle morphology. These results are consistent with previous theoretical and semi-empirical studies predicting frequent phase separation for particles in the SE-U.S.[89,90] Larger IEPOX:$Sulf_{inorg}$ ratios lead to thicker organic shells (e.g., laboratory mimic of Amazon) and can be correlated with the relatively larger amounts of particulate IEPOX-OS and corresponding oligomers (sum of OS corresponds to 27% of $Sulf_{inorg}$ in Figure 1A and 69% in Figure 1B). Hence, OS and oligomeric-OS may lead to a net modification of the morphology of the OA formed in the atmosphere.

As $Sulf_{inorg}$ is consumed and OSs are formed, the aerosol phase becomes more viscous and aerosol particle heights increase (Figure 3D). Height images and profiles from AFM were used as a proxy for liquid, semi-solid, or solid phase of the SOA, which is composed largely of an inorganic sulfate seed and organosulfur coating. The observation of more viscous aerosol is supported by the simulated viscosities of molecular tracers based on recent studies,[3,66] which suggest that IEPOX-derived OS has viscosity values 1–4 orders of magnitude higher than α-pinene SOA when the RH levels are below 70% (Figure 3D). Hence, IEPOX-derived OS can significantly increase the viscosity of aerosol particles, compared to isoprene-SOA compounds generated through self-nucleation in atmospheric simulation chambers under high concentrations without the addition of acidic sulfate particles.[91]

IEPOX-SOA volatility is significantly lower than structure-based vapor pressures of polyols predict,[92] which is consistent with the large inorganic-to-organic sulfate conversion reported here. Given the high modelled viscosity of IEPOX-OS and likely higher viscosity values of oligomeric-OS, the OS coating induced inhibition of multiphase chemistry would be larger than coatings of α-pinene SOA.[93] In the Amazon rainforest where average RH was higher than 80%, SOA particles were liquid, suggesting limited diffusion will not inhibit multiphase chemistry if RH>80%.[94] Even though the average RH is close to 80% for both the Amazon and SE-U.S., SI Figure S8 and previous measurements show that the median daytime RH in those regions is consistently below 70% (40–50% during the dry season in the Amazon) during the period of maximum diurnal IEPOX-SOA production.[93,95] Hence, diffusion of gaseous molecules limited by the formation of an OS coating will be more likely to affect multiphase chemistry during daytime in isoprene-rich environments, reducing heterogeneous SOA formation from compounds that are generated by photooxidation reactions.

Change in morphology is further supported by measuring the interfacial tension (IFT) depression of the major IEPOX-SOA products in microfluidic platform experiments. Surface tension and IFT are proxy measures of surface concentrations, as tensions will decrease with increased bulk-to-surface partitioning of surface-active components in the aqueous droplets. Each microfluidic measurement consumes 250–300 μL of aqueous solution, yielding 20–30 droplets. The IEPOX-OS droplet interfacial tensions reported in this work were statistically averaged and reported as the circle markers in Figure 4A. Additionally, Figures S2 and S9

show 2-methyltetrols and IEPOX-OS in methanol aqueous solution and 2-methyltetrols in pure water, respectively. IFT depression was observed in all cases (Figure 4A, Figure S2 and Figure S9), and IFT was lower when AS was present. In fact, lowering of the IFT in salty solutions indicates potential salting out [96,97] of the organics due to an enhancement of organic activity, driving more organic molecules to the surface. The salting out effect subsequently alters the SOA physicochemical properties by changing morphology to a core-shell structure rather than a homogeneously mixed sphere.[93] Salting out effects are quantified by combining the Setschenow equation and a two parameter surface and IFT model.[98] The Setschenow constant (K_s) indicates salting out when positive for organic-inorganic aqueous systems. The curves in Figure 4A shows model treatment for IEPOX-OS in pure water and in salty water and predicts that IEPOX-OS has a propensity for salting out in the presence of AS, which helps to explain the dependence of shell thickness on the ratio of IEPOX:$Sulf_{inorg}$. IEPOX-SOA may alter the climate properties of aerosols, for example, enhancing CCN activity by suppressing the surface tension to enhance cloud droplet formation from aerosols in organosulfur-rich particles, causing larger droplets to form before and during cloud activation.[99]

Figure 4B illustrates the limiting effects of IEPOX-SOA products on reactive uptake by aerosol which can most likely be ascribed to a slight decrease in acidity and transformation to a core-shell morphology as a result of the salting out effect induced by organosulfur compounds. The dramatic decrease of γ_{IEPOX} with increasing atmospheric-equivalent exposure time, highlights the profound modification of IEPOX-SOA on aerosol reactivity, explains the presence of residual IEPOX in the gas phase measured by CIMS (SI Figure S10), and the stabilization of $Sulf_{inorg}$ (Figures 1A and B) in our laboratory experiments. While previous studies have shown that other organic coatings tend to reduce multiphase chemical processes,[25,34,93] the results presented in Figure 4B provide direct evidence that uptake of IEPOX by sulfate aerosols has a self-limiting effect and indicate that the formation of a viscous IEPOX-SOA coating likely prevents further SOA formation in the ambient environment, primarily during daytime when RH is lower than 80%.

In sum, this study demonstrates that acid-driven multiphase chemistry of IEPOX converts a significant fraction of $Sulf_{inorg}$ to organosulfur within a range of IEPOX:$Sulf_{inorg}$ ratios relevant to most isoprene-dominated environments. We further demonstrate through laboratory and field measurements, the substantial conversion of sulfate, underlining the major role of IEPOX in controlling the chemical form of S(VI). Retrospective examination of field data in the SE-U.S. consistently shows that the contribution of organosulfur to S(VI) has been increasing with declining $Sulf_{inorg}$. The measured filter-based organosulfur fraction for Amazon, however, is not as much as that determined by the laboratory experiments conducted at the relevant ratios. There are two possible reasons. First, we conducted experiments mimicking both regions under the same initial condition of aerosol acidity and therefore the observed extent of conversion (up to ~90%) for Amazon relevant ratios likely represents the upper bound in the atmosphere. Second, collocated measurements of gas-phase IEPOX have rarely been reported for this area. The actual IEPOX:$Sulf_{inorg}$ could have been lower than the ratios tested in the laboratory mimic of Amazon. This also calls for the need to enrich the inventory of gas-phase IEPOX measurements to better constrain IEPOX:$Sulf_{inorg}$ in regions such as Amazon. From chamber experiments, the organosulfur

compounds are shown to impact aerosol acidity (up to 9 pH unit increase compared to the conventional case, where organosulfur compounds are not considered) by our thermodynamic model under assumptions similar to those widely used in models. A similar approach could be adopted in updating current thermodynamic models to assess this impact on predicting pH of ambient SOA. IEPOX reactive uptake results in a core-shell morphology supported by microscopic imaging and biphasic microfluidics. Through non-oxidative chemical processes, IEPOX-OS undergoes transformation to as yet uncharacterized organosulfur compounds, together with highly viscous IEPOX-OS, impeding further reactive uptake of IEPOX. Not examined in this work, though, is how the core-shell morphology may affect the prediction of aerosol acidity. It is obvious that the core and shell need to be treated separately in pH calculations. This warrants a systematic investigation in a future study. Worth noting is that the findings regarding IEPOX-OS and its implications for aerosol physicochemical properties have not been included in the presented global model for calculating the global IEPOX:$Sulf_{inorg}$. Overall the shift in sulfate distribution within aerosols, changing physicochemical properties, and decreasing multiphase reactivity caused by IEPOX multiphase chemistry have yet to be updated in the regional- and global-scale models to properly predict IEPOX-SOA formation and its impact on air quality and climate. In isoprene-dominated areas, IEPOX-OS, and potentially other biogenic/anthropogenic OS, likely govern the physicochemical properties of aerosol as well as the distribution of inorganic species such as sulfate or ammonium. Consequently, aerosol growth, multiphase reactions, including aging and reactive uptake of other species, and CCN activity change as surface tension, acidity, hygroscopicity and viscosity are modified. These changes could greatly impact atmospheric composition of biogenic SOA formed over isoprene-dominated areas. Hence, changes in SO_2 emissions at different locations around the world over time may have implications for the physicochemical properties of biogenic-derived SOA.

Supplementary Material

Refer to Web version on PubMed Central for supplementary material.

ACKNOWLEDGMENT

The authors wish to thank the Camille and Henry Dreyfus Postdoctoral Fellowship Program in Environmental Chemistry for their financial support. The authors would like to thank the Michigan Center for Materials Characterization for use and help with the SEM and the Banaszak-Holl lab for the use and help with the AFM. The contents of this publication are solely the responsibility of the authors and do not necessarily represent the official views of the U.S. Environmental Protection Agency (U.S. EPA). Further, the U.S. EPA does not endorse the purchase of any commercial products or services mentioned in the publication. The U.S. EPA through its Office of Research and Development collaborated in the research described here. It has been subjected to Agency administrative review and approved for publication but may not necessarily reflect official Agency policy. The authors wish to thank the IMPROVE network. IMPROVE is a collaborative association of state, tribal, and federal agencies, and international partners. U.S. EPA is the primary funding source, with contracting and research support from the National Park Service. The Air Quality Group at the University of California, Davis is the central analytical laboratory, with ion analysis provided by Research Triangle Institute, and carbon analysis provided by Desert Research Institute.

Funding Sources

This work is also funded in part by the U.S. EPA grant R835404, the National Science Foundation (NSF) grants AGS-1703535, AGS-1703019, AGS- 1554936, CHE-1404644 and CHE-1404573 and by the National Oceanic and Atmospheric Administration (NOAA) Climate Program Office’s AC4 program, award number NA13OAR4310064.

REFERENCES

(1). Jimenez JL; Canagaratna MR; Donahue NM; Prevot ASH; Zhang Q; Kroll JH; DeCarlo PF; Allan JD; Coe H; Ng NL; Aiken AC; Docherty KS; Ulbrich IM; Grieshop AP; Robinson AL; Duplissy J; Smith JD; Wilson KR; Lanz VA; Hueglin C; Sun YL; Tian J; Laaksonen A; Raatikainen T; Rautiainen J; Vaattovaara P; Ehn M; Kulmala M; Tomlinson JM; Collins DR; Cubison MJ; Dunlea J; Huffman JA; Onasch TB; Alfarra MR; Williams PI; Bower K; Kondo Y; Schneider J; Drewnick F; Borrmann S; Weimer S; Demerjian K; Salcedo D; Cottrell L; Griffin R; Takami A; Miyoshi T; Hatakeyama S; Shimono A; Sun JY; Zhang YM; Dzepina K; Kimmell R; Sueper D; Jayne JT; Herndon SC; Trimborn AM; Williams LR; Wood EC; Middlebrook AM; Kolb CE; Baltensperger U; Worsnop DR. Evolution of Organic Aerosols in the Atmosphere. Science 2009, 326 (5959), 1525–1529. 10.1126/science.1180353. [PubMed: 20007897]

(2). Pope III CA Lung Cancer, Cardiopulmonary Mortality, and Long-Term Exposure to Fine Particulate Air Pollution. JAMA 2002, 287 (9), 1132 10.1001/jama.287.9.1132. [PubMed: 11879110]

(3). Shiraiwa M; Li Y; Tsimpidi AP; Karydis VA; Berkemeier T; Pandis SN; Lelieveld J; Koop T; Pöschl U Global Distribution of Particle Phase State in Atmospheric Secondary Organic Aerosols. Nature Communications 2017, 8, 15002 10.1038/ncomms15002.

(4). Climate Change 2013 - The Physical Science Basis: Working Group I Contribution to the Fifth Assessment Report of the Intergovernmental Panel on Climate Change; Intergovernmental Panel on Climate Change, Ed.; Cambridge University Press: Cambridge, 2014 10.1017/CBO9781107415324.

(5). Surratt JD; Lewandowski M; Offenberg JH; Jaoui M; Kleindienst TE; Edney EO; Seinfeld JH Effect of Acidity on Secondary Organic Aerosol Formation from Isoprene. Environmental Science & Technology 2007, 41 (15), 5363–5369. 10.1021/es0704176. [PubMed: 17822103]

(6). Jang M Heterogeneous Atmospheric Aerosol Production by Acid-Catalyzed Particle-Phase Reactions. Science 2002, 298 (5594), 814–817. 10.1126/science.1075798. [PubMed: 12399587]

(7). Offenberg JH; Lewandowski M; Edney EO; Kleindienst TE; Jaoui M Influence of Aerosol Acidity on the Formation of Secondary Organic Aerosol from Biogenic Precursor Hydrocarbons. Environmental Science & Technology 2009, 43 (20), 7742–7747. 10.1021/es901538e. [PubMed: 19921888]

(8). Zhang H; Worton DR; Lewandowski M; Ortega J; Rubitschun CL; Park J-H; Kristensen K; Campuzano-Jost P; Day DA; Jimenez JL; Jaoui M; Offenberg JH; Kleindienst TE; Gilman J; Kuster WC; De Gouw J; Park C; Schade GW; Frossard AA; Russell L; Kaser L; Jud W; Hansel A; Cappellin L; Karl T; Glasius M; Guenther A; Goldstein AH; Seinfeld JH; Gold A; Kamens RM; Surratt JD Organosulfates as Tracers for Secondary Organic Aerosol (SOA) Formation from 2-Methyl-3-Buten-2-Ol (MBO) in the Atmosphere. Environmental Science & Technology 2012, 46 (17), 9437–9446. 10.1021/es301648z. [PubMed: 22849588]

(9). He K; Yang F; Ma Y; Zhang Q; Yao X; Chan CK; Cadle S; Chan T; Mulawa P The Characteristics of PM2.5 in Beijing, China. Atmospheric Environment 2001, 35 (29), 4959–4970. 10.1016/S1352-2310(01)00301-6.

(10). Wu Y; Hao J; Fu L; Hu J; Wang Z; Tang U Chemical Characteristics of Airborne Particulate Matter near Major Roads and at Background Locations in Macao, China. The Science of The Total Environment 2003, 317 (1–3), 159–172. 10.1016/S0048-9697(03)00331-0. [PubMed: 14630419]

(11). Lukács H; Gelencsér A; Hoffer A; Kiss G; Horváth K; Hartyáni Z Quantitative Assessment of Organosulfates in Size-Segregated Rural Fine Aerosol. Atmospheric Chemistry and Physics 2009, 9 (1), 231–238. 10.5194/acp-9-231-2009.

(12). Tolocka MP; Turpin B Contribution of Organosulfur Compounds to Organic Aerosol Mass. Environmental Science & Technology 2012, 46 (15), 7978–7983. 10.1021/es300651v. [PubMed: 22731120]

(13). Shakya KM; Peltier RE Non-Sulfate Sulfur in Fine Aerosols across the United States: Insight for Organosulfate Prevalence. Atmospheric Environment 2015, 100, 159–166. 10.1016/j.atmosenv.2014.10.058. [PubMed: 25620874]

(14). Pratt KA; Fiddler MN; Shepson PB; Carlton AG; Surratt JD Organosulfates in Cloud Water above the Ozarks' Isoprene Source Region. Atmospheric Environment 2013, 77, 231–238. 10.1016/j.atmosenv.2013.05.011.

(15). Boone EJ; Laskin A; Laskin J; Wirth C; Shepson PB; Stirm BH; Pratt KA Aqueous Processing of Atmospheric Organic Particles in Cloud Water Collected via Aircraft Sampling. Environmental Science & Technology 2015, 49 (14), 8523–8530. 10.1021/acs.est.5b01639. [PubMed: 26068538]

(16). Altieri KE; Turpin BJ; Seitzinger SP Oligomers, Organosulfates, and Nitrooxy Organosulfates in Rainwater Identified by Ultra-High Resolution Electrospray Ionization FT-ICR Mass Spectrometry. Atmospheric Chemistry and Physics 2009, 9 (7), 2533–2542. 10.5194/acp-9-2533-2009.

(17). Gómez-González Y; Surratt JD; Cuyckens F; Szmigielski R; Vermeylen R; Jaoui M; Lewandowski M; Offenberg JH; Kleindienst TE; Edney EO; Blockhuys F; Van Alsenoy C; Maenhaut W; Claeys M Characterization of Organosulfates from the Photooxidation of Isoprene and Unsaturated Fatty Acids in Ambient Aerosol Using Liquid Chromatography/(−) Electrospray Ionization Mass Spectrometry. Journal of Mass Spectrometry 2008, 43 (3), 371–382. 10.1002/jms.1329. [PubMed: 17968849]

(18). Hawkins LN; Russell LM; Covert DS; Quinn PK; Bates TS Carboxylic Acids, Sulfates, and Organosulfates in Processed Continental Organic Aerosol over the Southeast Pacific Ocean during VOCALS-REx 2008. Journal of Geophysical Research 2010, 115 (D13). 10.1029/2009JD013276.

(19). Hansen AMK; Kristensen K; Nguyen QT; Zare A; Cozzi F; Nøjgaard JK; Skov H; Brandt J; Christensen JH; Ström J; Tunved P; Krejci R; Glasius M Organosulfates and Organic Acids in Arctic Aerosols: Speciation, Annual Variation and Concentration Levels. Atmospheric Chemistry and Physics 2014, 14 (15), 7807–7823. 10.5194/acp-14-7807-2014.

(20). Glasius M; Bering MS; Yee L; de Sá S; Isaacman-VanWertz G; Wernis RA; Barbosa HMJ; Alexander ML; Palm BB; Hu WW; Campuzano-Jost P; Day DA; Jimenez JL; Shrivastava M; Scot MT; Goldstein AH Organosulfates in aerosols downwind of an urban region in central Amazon. Environmental Science: Processes and Impacts 2018, 20 (11), 1546–1558. [PubMed: 30357193]

(21). Weber RJ; Guo H; Russell AG; Nenes A High Aerosol Acidity despite Declining Atmospheric Sulfate Concentrations over the Past 15 Years. Nature Geoscience 2016, 9 (4), 282–285. 10.1038/ngeo2665.

(22). Bates KH; Crounse JD; Clair JM St.; Bennett NB; Nguyen TB; Seinfeld JH; Stoltz BM; Wennberg PO Gas Phase Production and Loss of Isoprene Epoxydiols. The Journal of Physical Chemistry A 2014, 118 (7), 1237–1246. 10.1021/jp4107958. [PubMed: 24476509]

(23). Paulot F; Crounse JD; Kjaergaard HG; Kurten A St. Clair JM; Seinfeld JH; Wennberg PO Unexpected Epoxide Formation in the Gas-Phase Photooxidation of Isoprene. Science 2009, 325 (5941), 730–733. 10.1126/science.1172910. [PubMed: 19661425]

(24). Surratt JD; Chan AWH; Eddingsaas NC; Chan M; Loza CL; Kwan AJ; Hersey SP; Flagan RC; Wennberg PO; Seinfeld JH Reactive Intermediates Revealed in Secondary Organic Aerosol Formation from Isoprene. Proceedings of the National Academy of Sciences 2010, 107 (15), 6640–6645. 10.1073/pnas.0911114107.

(25). Gaston CJ; Riedel TP; Zhang Z; Gold A; Surratt JD; Thornton JA Reactive Uptake of an Isoprene-Derived Epoxydiol to Submicron Aerosol Particles. Environmental Science & Technology 2014, 48 (19), 11178–11186. 10.1021/es5034266. [PubMed: 25207961]

(26). Rattanavaraha W; Chu K; Budisulistiorini SH; Riva M; Lin Y-H; Edgerton ES; Baumann K; Shaw SL; Guo H; King L; Weber RJ; Neff ME; Stone EA; Offenberg JH; Zhang Z; Gold A; Surratt JD Assessing the Impact of Anthropogenic Pollution on Isoprene-Derived Secondary Organic Aerosol Formation in PM2.5 Collected from the Birmingham, Alabama, Ground Site during the 2013 Southern Oxidant and Aerosol Study. Atmospheric Chemistry and Physics 2016, 16 (8), 4897–4914. 10.5194/acp-16-4897-2016.

(27). Budisulistiorini SH; Li X; Bairai ST; Renfro J; Liu Y; Liu YJ; McKinney KA; Martin ST; McNeill VF; Pye HOT; Nenes A; Neff ME; Stone EA; Mueller S; Knote C; Shaw SL; Zhang Z; Gold A; Surratt JD Examining the Effects of Anthropogenic Emissions on Isoprene-Derived

Secondary Organic Aerosol Formation during the 2013 Southern Oxidant and Aerosol Study (SOAS) at the Look Rock, Tennessee Ground Site. Atmospheric Chemistry and Physics 2015, 15 (15), 8871–8888. 10.5194/acp-15-8871-2015.

(28). Hu WW; Campuzano-Jost P; Palm BB; Day DA; Ortega AM; Hayes PL; Krechmer JE; Chen Q; Kuwata M; Liu YJ; de Sá SS; Martin ST; Hu M; Budisulistiorini SH; Riva M; Surratt JD; Clair JM St.; Isaacman-Van Wertz G; Yee LD; Goldstein AH; Carbone S; Artaxo P; de Gouw JA; Koss A; Wisthaler A; Mikoviny T; Karl T; Kaser L; Jud W; Hansel A; Docherty KS; Canagaratna MR; Paulot F; Jimenez JL Characterization of a Real-Time Tracer for Isoprene Epoxydiols-Derived Secondary Organic Aerosol (IEPOX-SOA) from Aerosol Mass Spectrometer Measurements. Atmospheric Chemistry and Physics 2015, 15 (20), 11807–11833. 10.5194/acp-15-11807-2015.

(29). Robinson NH; Newton HM; Allan JD; Irwin M; Hamilton JF; Flynn M; Bower KN; Williams PI; Mills G; Reeves CE; McFiggans G; and Coe H Evidence for a Significant Proportion of Secondary Organic Aerosol from Isoprene above a Maritime Tropical Forest. Atmospheric Chemistry and Physics 2011, 11 (3), 1039–1050. 10.5194/acp-11-1039-2011.

(30). Xu L; Guo H; Boyd CM; Klein M; Bougiatioti A; Cerully KM; Hite JR; Isaacman-VanWertz G; Kreisberg NM; Knote C; Olson K; Koss A; Goldstein AH; Hering SV; De Gouw J; Baumann K; Lee S-H; Nenes A; Weber RJ; Ng NL Effects of Anthropogenic Emissions on Aerosol Formation from Isoprene and Monoterpenes in the Southeastern United States. Proceedings of the National Academy of Sciences 2015, 112 (1), 37–42. 10.1073/pnas.1417609112.

(31). de Sá SS; Palm BB; Campuzano-Jost P; Day DA; Newburn MK; Hu W; Isaacman-VanWertz G; Yee LD; Thalman R; Brito J; Carbone S; Artaxo P; Goldstein AH; Manzi AO; Souza RAF; Mei F; Shilling JE; Springston SR; Wang J; Surratt JD; Alexander ML; Jimenez JL; Martin ST Influence of Urban Pollution on the Production of Organic Particulate Matter from Isoprene Epoxydiols in Central Amazonia. Atmospheric Chemistry and Physics 2017, 17 (11), 6611–6629. 10.5194/acp-17-6611-2017.

(32). Surratt JD; Gómez-González Y; Chan AWH; Vermeylen R; Shahgholi M; Kleindienst TE; Edney EO; Offenberg JH; Lewandowski M; Jaoui M; Maenhaut W; Claeys M; Flagan RC; Seinfeld JH Organosulfate Formation in Biogenic Secondary Organic Aerosol. The Journal of Physical Chemistry A 2008, 112 (36), 8345–8378. 10.1021/jp802310p. [PubMed: 18710205]

(33). Lin Y-H; Zhang Z; Docherty KS; Zhang H; Budisulistiorini SH; Rubitschun CL; Shaw SL; Knipping EM; Edgerton ES; Kleindienst TE; Gold A; Surratt JD Isoprene Epoxydiols as Precursors to Secondary Organic Aerosol Formation: Acid-Catalyzed Reactive Uptake Studies with Authentic Compounds. Environmental Science & Technology 2012, 46 (1), 250–258. 10.1021/es202554c. [PubMed: 22103348]

(34). Riva M; Bell DM; Hansen A-MK; Drozd GT; Zhang Z; Gold A; Imre D; Surratt JD; Glasius M; Zelenyuk A Effect of Organic Coatings, Humidity and Aerosol Acidity on Multiphase Chemistry of Isoprene Epoxydiols. Environmental Science & Technology 2016, 50 (11), 5580–5588. 10.1021/acs.est.5b06050. [PubMed: 27176464]

(35). Riva M; Budisulistiorini SH; Zhang Z; Gold A; Surratt JD Chemical Characterization of Secondary Organic Aerosol Constituents from Isoprene Ozonolysis in the Presence of Acidic Aerosol. Atmospheric Environment 2016, 130, 5–13. 10.1016/j.atmosenv.2015.06.027.

(36). Zhang Z; Lin Y-H; Zhang H; Surratt JD; Ball LM; Gold A Technical Note: Synthesis of Isoprene Atmospheric Oxidation Products: Isomeric Epoxydiols and the Rearrangement Products *Cis*- and *Trans*-3-Methyl-3,4-Dihydroxytetrahydrofuran. Atmospheric Chemistry and Physics 2012, 12 (18), 8529–8535. 10.5194/acp-12-8529-2012.

(37). Riedel TP; Lin Y-H; Budisulistiorini SH; Gaston CJ; Thornton JA; Zhang Z; Vizuete W; Gold A; Surratt JD Heterogeneous Reactions of Isoprene-Derived Epoxides: Reaction Probabilities and Molar Secondary Organic Aerosol Yield Estimates. Environmental Science & Technology Letters 2015, 2 (2), 38–42. 10.1021/ez500406f.

(38). Riedel TP; Lin Y-H; Zhang Z; Chu K; Thornton JA; Vizuete W; Gold A; Surratt JD Constraining Condensed-Phase Formation Kinetics of Secondary Organic Aerosol Components from Isoprene Epoxydiols. Atmospheric Chemistry and Physics 2016, 16 (3), 1245–1254. 10.5194/acp-16-1245-2016.

(39). Martin ST; Artaxo P; Machado LAT; Manzi AO; Souza RAF; Schumacher C; Wang J; Andreae MO; Barbosa HMJ; Fan J; Fish G; Goldstein AH; Guenther A; Jimenez JL, Pöschl U; Silva Dias

MA; Smith JN; Wendisch M Introduction: Observations and Modeling of the Green Ocean Amazon (GoAmazon2014/5). Introduction: Observations and Modeling of the Green Ocean Amazon (GoAmazon2014/5). Atmospheric Chemistry and Physics 2016, 16 (8), 4785–4797. 10.5194/acp-16-4785-2016.

(40). Lin Y-H; Budisulistiorini SH; Chu K; Siejack RA; Zhang H; Riva M; Zhang Z; Gold A; Kautzman KE; Surratt JD Light-Absorbing Oligomer Formation in Secondary Organic Aerosol from Reactive Uptake of Isoprene Epoxydiols. Environmental Science & Technology 2014, 48 (20), 12012–12021. 10.1021/es503142b. [PubMed: 25226366]

(41). Riva M; Budisulistiorini SH; Chen Y; Zhang Z; D'Ambro EL; Zhang X; Gold A; Turpin BJ; Thornton JA; Canagaratna MR; Surratt JD Chemical Characterization of Secondary Organic Aerosol from Oxidation of Isoprene Hydroxyhydroperoxides. Environmental Science & Technology 2016, 50 (18), 9889–9899. 10.1021/acs.est.6b02511. [PubMed: 27466979]

(42). Malm WC; Sisler JF; Huffman D; Eldred RA; Cahill TA Spatial and Seasonal Trends in Particle Concentration and Optical Extinction in the United States. Journal of Geophysical Research 1994, 99 (D1), 1347 10.1029/93JD02916.

(43). Ault AP; Axson JL Atmospheric Aerosol Chemistry: Spectroscopic and Microscopic Advances. Analytical Chemistry 2017, 89 (1), 430–452. 10.1021/acs.analchem.6b04670. [PubMed: 28105816]

(44). Bondy AL; Kirpes RM; Merzel RL; Pratt KA; Banaszak Holl MM; Ault AP Atomic Force Microscopy-Infrared Spectroscopy of Individual Atmospheric Aerosol Particles: Subdiffraction Limit Vibrational Spectroscopy and Morphological Analysis. Anal. Chem 2017, 89 (17), 8594–8598. 10.1021/acs.analchem.7b02381. [PubMed: 28813142]

(45). Bondy AL; Wang B; Laskin A; Craig RL; Nhliziyo MV; Bertman SB; Pratt KA; Shepson PB; Ault AP Inland Sea Spray Aerosol Transport and Incomplete Chloride Depletion: Varying Degrees of Reactive Processing Observed during SOAS. Environ. Sci. Technol 2017, 51 (17), 9533–9542. 10.1021/acs.est.7b02085. [PubMed: 28732168]

(46). Metcalf AR; Boyer HC; Dutcher CS Interfacial Tensions of Aged Organic Aerosol Particle Mimics Using a Biphasic Microfluidic Platform. Environmental Science & Technology 2016, 50 (3), 1251–1259. 10.1021/acs.est.5b04880. [PubMed: 26713671]

(47). Hudson SD; Cabral JT; Goodrum WJ; Beers KL; Amis EJ Microfluidic Interfacial Tensiometry. Applied Physics Letters 2005, 87 (8), 081905 10.1063/1.2034098.

(48). Cabral JT; Hudson SD Microfluidic Approach for Rapid Multicomponent Interfacial Tensiometry. Lab on a Chip 2006, 6 (3), 427 10.1039/b511976f. [PubMed: 16511627]

(49). Lee D; Fang C; Ravan AS; Fuller GG; Shen AQ Temperature Controlled Tensiometry Using Droplet Microfluidics. Lab on a Chip 2017, 17 (4), 717–726. 10.1039/C6LC01384H. [PubMed: 28154859]

(50). Narayan S; Moravec DB; Hauser BG; Dallas AJ; Dutcher CS Removing Water from Diesel Fuel: Understanding the Impact of Droplet Size on Dynamic Interfacial Tension of Water-in-Fuel Emulsions. Energy & Fuels 2018, 32 (7), 7326–7337. 10.1021/acs.energyfuels.8b00502.

(51). Metcalf AR; Narayan S; Dutcher CS A Review of Microfluidic Concepts and Applications for Atmospheric Aerosol Science. Aerosol Science and Technology 2018, 52 (3), 310–329. 10.1080/02786826.2017.1408952.

(52). Mazutis L; Gilbert J; Ung WL; Weitz DA; Griffiths AD; Heyman JA Single-Cell Analysis and Sorting Using Droplet-Based Microfluidics. Nature Protocols 2013, 8 (5), 870–891. 10.1038/nprot.2013.046. [PubMed: 23558786]

(53). Qin D; Xia Y; Whitesides GM Soft Lithography for Micro- and Nanoscale Patterning. Nature Protocols 2010, 5 (3), 491–502. 10.1038/nprot.2009.234. [PubMed: 20203666]

(54). Xia Y; Whitesides GM Soft Lithography. Angewandte Chemie International Edition 1998, 37 (5), 550–575. 10.1002/(SICI)1521-3773(19980316)37:5<550::AID-ANIE550>3.0.CO;2-G. [PubMed: 29711088]

(55). Anna SL; Bontoux N; Stone HA Formation of Dispersions Using "Flow Focusing" in Microchannels. Applied Physics Letters 2003, 82 (3), 364–366. 10.1063/1.1537519.

(56). Garstecki P; Gitlin I; DiLuzio W; Whitesides GM; Kumacheva E; Stone HA Formation of Monodisperse Bubbles in a Microfluidic Flow-Focusing Device. Applied Physics Letters 2004, 85 (13), 2649–2651. 10.1063/1.1796526.

(57). Moyle TM; Walker LM; Anna SL Predicting Conditions for Microscale Surfactant Mediated Tipstreaming. Physics of Fluids 2012, 24 (8), 082110 10.1063/1.4746253.

(58). Rallison JM The Deformation of Small Viscous Drops and Bubbles in Shear Flows. Annual Review of Fluid Mechanics 1984, 16 (1), 45–66. 10.1146/annurev.fl.16.010184.000401.

(59). Taylor GI The Formation of Emulsions in Definable Fields of Flow. Proceedings of the Royal Society A: Mathematical, Physical and Engineering Sciences 1934, 146 (858), 501–523. 10.1098/rspa.1934.0169.

(60). Taylor GI The Viscosity of a Fluid Containing Small Drops of Another Fluid. Proceedings of the Royal Society A: Mathematical, Physical and Engineering Sciences 1932, 138 (834), 41–48. 10.1098/rspa.1932.0169.

(61). Martin JD; Hudson SD Mass Transfer and Interfacial Properties in Two-Phase Microchannel Flows. New Journal of Physics 2009, 11 (11), 115005 10.1088/1367-2630/11/11/115005.

(62). Laliberté M A Model for Calculating the Heat Capacity of Aqueous Solutions, with Updated Density and Viscosity Data. Journal of Chemical & Engineering Data 2009, 54 (6), 1725–1760. 10.1021/je8008123.

(63). Boyer HC; Dutcher CS Atmospheric Aqueous Aerosol Surface Tensions: Isotherm-Based Modeling and Biphasic Microfluidic Measurements. J. Phys. Chem. A 2017, 121 (25), 4733–4742. 10.1021/acs.jpca.7b03189. [PubMed: 28498664]

(64). Angell CA Formation of Glasses from Liquids and Biopolymers. Science 1995, 267 (5206), 1924–1935. 10.1126/science.267.5206.1924. [PubMed: 17770101]

(65). Angell CA Liquid Fragility and the Glass Transition in Water and Aqueous Solutions. Chemical Reviews 2002, 102 (8), 2627–2650. 10.1021/cr000689q. [PubMed: 12175262]

(66). DeRieux W-SW; Li Y; Lin P; Laskin J; Laskin A; Bertram AK; Nizkorodov SA; Shiraiwa M Predicting the Glass Transition Temperature and Viscosity of Secondary Organic Material Using Molecular Composition. Atmospheric Chemistry and Physics 2018, 18 (9), 6331–6351. 10.5194/acp-18-6331-2018.

(67). Fountoukis C; Nenes A ISORROPIA II: A Computationally Efficient Thermodynamic Equilibrium Model for K^+–Ca^{2+}–Mg^{2+}–NH_4^+–Na^+–SO_4^{2-}–NO_3^-;–Cl^-–H_2O Aerosols. Atmospheric Chemistry and Physics 2007, 7 (17), 4639–4659. 10.5194/acp-7-4639-2007.

(68). Szopa S; Balkanski Y; Schulz M; Bekki S; Cugnet D; Fortems-Cheiney A; Turquety S; Cozic A; Déandreis C; Hauglustaine D; Idelkadi A; Lathière J; Lefevre F; Marchand M; Vuolo R; Yan N; Dufresne J,-L Aerosol and Ozone Changes as Forcing for Climate Evolution between 1850 and 2100. Climate Dynamics 2013, 40 (9–10), 2223–2250. 10.1007/s00382-012-1408-y.

(69). Clair JM St.; Rivera-Rios JC; Crounse JD; Knap HC; Bates KH; Teng AP; Jørgensen S; Kjaergaard HG; Keutsch FN; Wennberg PO Kinetics and Products of the Reaction of the First-Generation Isoprene Hydroxy Hydroperoxide (ISOPOOH) with OH. The Journal of Physical Chemistry A 2016, 120 (9), 1441–1451. 10.1021/acs.jpca.5b06532. [PubMed: 26327174]

(70). Riahi K; Grübler A; Nakicenovic N Scenarios of Long-Term Socio-Economic and Environmental Development under Climate Stabilization. Technological Forecasting and Social Change 2007, 74 (7), 887–935. 10.1016/j.techfore.2006.05.026.

(71). Messina P; Lathière J; Sindelarova K; Vuichard N; Granier C; Ghattas J; Cozic A; Hauglustaine DA Global Biogenic Volatile Organic Compound Emissions in the ORCHIDEE and MEGAN Models and Sensitivity to Key Parameters. Atmospheric Chemistry and Physics 2016, 16 (22), 14169–14202. 10.5194/acp-16-14169-2016.

(72). Nguyen TB; Coggon MM; Bates KH; Zhang X; Schwantes RH; Schilling KA; Loza CL; Flagan RC; Wennberg PO; Seinfeld JH Organic Aerosol Formation from the Reactive Uptake of Isoprene Epoxydiols (IEPOX) onto Non-Acidified Inorganic Seeds. Atmospheric Chemistry and Physics 2014, 14 (7), 3497–3510. 10.5194/acp-14-3497-2014.

(73). Piletic IR; Edney EO; Bartolotti LJ A Computational Study of Acid Catalyzed Aerosol Reactions of Atmospherically Relevant Epoxides. Physical Chemistry Chemical Physics 2013, 15 (41), 18065 10.1039/c3cp52851k. [PubMed: 24061334]

(74). Xing J; Mathur R; Pleim J; Hogrefe C; Gan C-M; Wong DC; Wei C; Gilliam R; Pouliot G Observations and Modeling of Air Quality Trends over 1990–2010 across the Northern Hemisphere: China, the United States and Europe. Atmospheric Chemistry and Physics 2015, 15 (5), 2723–2747. 10.5194/acp-15-2723-2015.

(75). Attwood AR; Washenfelder RA; Brock CA; Hu W; Baumann K; Campuzano-Jost P; Day DA; Edgerton ES; Murphy DM; Palm BB; McComiskey A; Wagner NL; de Sá SS; Ortega A; Martin ST; Jimenez JL; Brown SS Trends in Sulfate and Organic Aerosol Mass in the Southeast U.S.: Impact on Aerosol Optical Depth and Radiative Forcing: Aerosol Mass and Optical Depth in SE US. Geophysical Research Letters 2014, 41 (21), 7701–7709. 10.1002/2014GL061669.

(76). Hand JL; Schichtel BA; Malm WC; Pitchford ML Particulate Sulfate Ion Concentration and SO_2 Emission Trends in the United States from the Early 1990s through 2010. Atmospheric Chemistry and Physics 2012, 12 (21), 10353–10365. 10.5194/acp-12-10353-2012.

(77). Déandreis C; Balkanski Y; Dufresne JL; Cozic A Radiative Forcing Estimates of Sulfate Aerosol in Coupled Climate-Chemistry Models with Emphasis on the Role of the Temporal Variability. Atmospheric Chemistry and Physics 2012, 12 (12), 5583–5602. 10.5194/acp-12-5583-2012.

(78). Shindell DT; Lamarque J-F; Schulz M; Flanner M; Jiao C; Chin M; Young PJ; Lee YH; Rotstayn L; Mahowald N; Milly G; Faluvegi G; Balkanski Y; Collins WJ; Conley AJ; Dalsoren S; Easter R; Ghan S; Horowitz L; Liu X; Myhre G; Nagashima T; Naik V; Rumbold ST; Skeie R; Sudo K; Szopa S; Takemura T; Voulgarakis A; Yoon J-H; Lo F Radiative Forcing in the ACCMIP Historical and Future Climate Simulations. Atmospheric Chemistry and Physics 2013, 13 (6), 2939–2974. 10.5194/acp-13-2939-2013.

(79). Young PJ; Archibald AT; Bowman KW; Lamarque J-F; Naik V; Stevenson DS; Tilmes S; Voulgarakis A; Wild O; Bergmann D; Cameron-Smith P; Cionni I; Collins WJ; Dalsøren SB; Doherty RM; Eyring V; Faluvegi G; Horowitz LW; Josse B; Lee YH; MacKenzie IA; Nagashima T; Plummer DA; Righi M; Rumbold ST; Skeie RB; Shindell DT; Strode SA; Sudo K; Szopa S; Zeng G Pre-Industrial to End 21st Century Projections of Tropospheric Ozone from the Atmospheric Chemistry and Climate Model Intercomparison Project (ACCMIP). Atmospheric Chemistry and Physics 2013, 13 (4), 2063–2090. 10.5194/acp-13-2063-2013.

(80). Nguyen QT; Christensen MK; Cozzi F; Zare A; Hansen AMK; Kristensen K; Tulinius TE; Madsen HH; Christensen JH; Brandt J; Massling A; Nøjgaard JK; Glasius M Understanding the Anthropogenic Influence on Formation of Biogenic Secondary Organic Aerosols in Denmark via Analysis of Organosulfates and Related Oxidation Products. Atmospheric Chemistry and Physics 2014, 14 (17), 8961–8981. 10.5194/acp-14-8961-2014.

(81). Hettiyadura APS; Jayarathne T; Baumann K; Goldstein AH; de Gouw JA; Koss A; Keutsch FN; Skog K; Stone EA Qualitative and Quantitative Analysis of Atmospheric Organosulfates in Centreville, Alabama. Atmospheric Chemistry and Physics 2017, 17 (2), 1343–1359. 10.5194/acp-17-1343-2017.

(82). Huang DD; Li YJ; Lee BP; Chan CK Analysis of Organic Sulfur Compounds in Atmospheric Aerosols at the HKUST Supersite in Hong Kong Using HR-ToF-AMS. Environmental Science & Technology 2015, 49 (6), 3672–3679. 10.1021/es5056269. [PubMed: 25700022]

(83). Kaiser J; Skog KM; Baumann K; Bertman SB; Brown SB; Brune WH; Crounse JD; de Gouw JA; Edgerton ES; Feiner PA; Goldstein AH; Koss A; Misztal PK; Nguyen TB; Olson KF; Clair JM St.; Teng AP; Toma S; Wennberg PO; Wild RJ; Zhang L; Keutsch FN Speciation of OH Reactivity above the Canopy of an Isoprene-Dominated Forest. Atmospheric Chemistry and Physics 2016, 16 (14), 9349–9359. 10.5194/acp-16-9349-2016.

(84). Weber RJ; Guo H; Russell AG; Nenes A High Aerosol Acidity despite Declining Atmospheric Sulfate Concentrations over the Past 15 Years. Nature Geoscience 2016, 9 (4), 282–285. 10.1038/ngeo2665.

(85). Fountoukis C; Nenes A; Sullivan A; Weber R; Van Reken T; Fischer M; Matías E; Moya M; Farmer D; Cohen RC Thermodynamic Characterization of Mexico City Aerosol during MILAGRO 2006. Atmospheric Chemistry and Physics 2009, 9 (6), 2141–2156. 10.5194/acp-9-2141-2009.

(86). Clegg SL; Brimblecombe P; Wexler AS Thermodynamic Model of the System H^+ –NH_4^+ –SO_4^{2-} –NO_3^-–H_2O at Tropospheric Temperatures. The Journal of Physical Chemistry A 1998, 102 (12), 2137–2154. 10.1021/jp973042r.

(87). Zuend A; Marcolli C; Luo BP; Peter T A Thermodynamic Model of Mixed Organic-Inorganic Aerosols to Predict Activity Coefficients. Atmospheric Chemistry and Physics 2008, 8 (16), 4559–4593. 10.5194/acp-8-4559-2008.

(88). Slade JH; Ault AP; Bui AT; Ditto JC; Lei Z; Bondy AL; Olson NE; Cook RD; Desrochers SJ; Harvey RM; Erickson MH; Wallace HW; Alvarez SL; Flynn JH; Boor BE; Petrucci GA; Gentner DR; Griffin RJ; Shepson PB Bouncier Particles at Night: Biogenic Secondary Organic Aerosol Chemistry and Sulfate Drive Diel Variations in the Aerosol Phase in a Mixed Forest. Environ. Sci. Technol 2019 10.1021/acs.est.8b07319.

(89). Pye HOT; Zuend A; Fry JL; Isaacman-VanWertz G; Capps SL; Appel KW; Foroutan H; Xu L; Ng NL; Goldstein AH Coupling of Organic and Inorganic Aerosol Systems and the Effect on Gas&Ndash;Particle Partitioning in the Southeastern US. Atmospheric Chemistry and Physics 2018, 18 (1), 357–370. 10.5194/acp-18-357-2018. [PubMed: 29963078]

(90). Pye HOT; Murphy BN; Xu L; Ng NL; Carlton AG; Guo H; Weber R; Vasilakos P; Appel KW; Budisulistiorini SH; Surratt JD; Nenes A; Hu WW; Jimenez JL; Isaacman-VanWertz G; Misztal PK; Goldstein AH On the Implications of Aerosol Liquid Water and Phase Separation for Organic Aerosol Mass. Atmospheric Chemistry and Physics 2017, 17 (1), 343–369. 10.5194/acp-17-343-2017. [PubMed: 30147709]

(91). Song M; Liu PF; Hanna SJ; Li YJ; Martin ST; Bertram AK Relative Humidity-Dependent Viscosities of Isoprene-Derived Secondary Organic Material and Atmospheric Implications for Isoprene-Dominant Forests. Atmospheric Chemistry and Physics 2015, 15 (9), 5145–5159. 10.5194/acp-15-5145-2015.

(92). Lopez-Hilfiker FD; Mohr C; D'Ambro EL; Lutz A; Riedel TP; Gaston CJ; Iyer S; Zhang Z; Gold A; Surratt JD; Lee BH; Kurten T; Hu WW; Jimenez JL; Hallquist M; Thornton JA Molecular Composition and Volatility of Organic Aerosol in the Southeastern U.S.: Implications for IEPOX Derived SOA. Environmental Science & Technology 2016, 50 (5), 2200–2209. 10.1021/acs.est.5b04769. [PubMed: 26811969]

(93). Zhang Y; Chen Y; Lambe AT; Olson NE; Lei Z; Craig RL; Zhang Z; Gold A; Onasch TB; Jayne JT; Worsnop DR; Gaston CJ; Thornton JA; Vizuete W; Ault A; Surratt JD Effect of the Aerosol-Phase State on Secondary Organic Aerosol Formation from the Reactive Uptake of Isoprene-Derived Epoxydiols (IEPOX). Environmental Science & Technology Letters 2018, 5 (3), 167–174. 10.1021/acs.estlett.8b00044.

(94). Bateman AP; Gong Z; Liu P; Sato B; Cirino G; Zhang Y; Artaxo P; Bertram AK; Manzi AO; Rizzo LV; Souza RAF; Zaveri RA; Martin ST Sub-Micrometre Particulate Matter Is Primarily in Liquid Form over Amazon Rainforest. Nature Geoscience 2016, 9 (1), 34–37. 10.1038/ngeo2599.

(95). Guo H; Xu L; Bougiatioti A; Cerully KM; Capps SL; Hite JR; Carlton AG; Lee S-H; Bergin MH; Ng NL; Nenes A; Weber RJ Fine-Particle Water and PH in the Southeastern United States. Atmospheric Chemistry and Physics 2015, 15 (9), 5211–5228. 10.5194/acp-15-5211-2015.

(96). Wang C; Lei YD; Endo S; Wania F Measuring and Modeling the Salting-out Effect in Ammonium Sulfate Solutions. Environ. Sci. Technol 2014, 48 (22), 13238–13245. 10.1021/es5035602. [PubMed: 25321609]

(97). Bertram AK; Martin ST; Hanna SJ; Smith ML; Bodsworth A; Chen Q; Kuwata M; Liu A; You Y; Zorn SR Predicting the Relative Humidities of Liquid-Liquid Phase Separation, Efflorescence, and Deliquescence of Mixed Particles of Ammonium Sulfate, Organic Material, and Water Using the Organic-to-Sulfate Mass Ratio of the Particle and the Oxygen-to-Carbon Elemental Ratio of the Organic Component. Atmospheric Chemistry and Physics 2011, 11 (21), 10995–11006.

(98). Wexler AS; Dutcher CS Statistical Mechanics of Multilayer Sorption: Surface Tension. Journal of Physical Chemistry Letters 2013, 4 (10), 1723–1726. 10.1021/jz400725p. [PubMed: 26282984]

(99). Ruehl CR; Davies JF; Wilson KR An Interfacial Mechanism for Cloud Droplet Formation on Organic Aerosols. Science 2016, 351 (6280), 1447–1450. 10.1126/science.aad4889. [PubMed: 27013731]

(100). Metcalf AR; Boyer HC; Dutcher CS Interfacial Tensions of Aged Organic Aerosol Particle Mimics Using a Biphasic Microfluidic Platform. Environmental Science & Technology 2016, 50 (3), 1251–1259. 10.1021/acs.est.5b04880. [PubMed: 26713671]

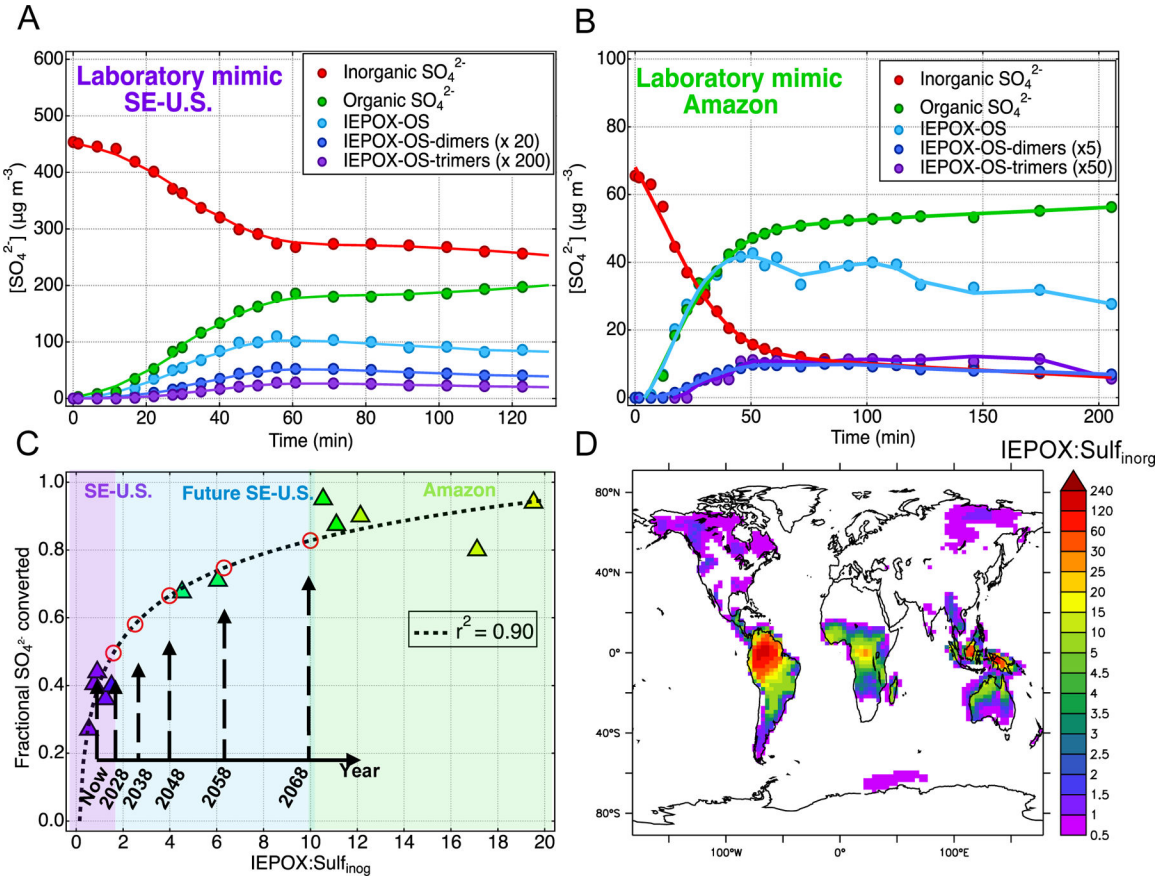

Figure 1.

Laboratory conversion (RH=50%) of $Sulf_{inorg}$ to organic sulfate during the reactive uptake of IEPOX at IEPOX (μg m^{-3}):$Sulf_{inorg}$ (μg m^{-3}) ratios atmospherically relevant to (A) a laboratory mimic of the SE-U.S. (ratio=1.5) and (B) a laboratory mimic of the Amazon (ratio=17.1). IEPOX is injected into the chamber at t = 0 and stopped at t = 60. IEPOX-OS dimer and trimer concentrations are shown on and expanded scale for clarity. (C) Filled triangular markers indicate the conversion of $Sulf_{inorg}$ to organic sulfate as a function of IEPOX:$Sulf_{inorg}$ in chamber experiments at RH~50%. Colors correspond to those in Figure 1D. Red open circles correspond to projected IEPOX:$Sulf_{inorg}$ over the next 50 years, based on $Sulf_{inorg}$ reduction rates from Attwood et al.[75] and Hand et al.[76], and assuming constant IEPOX. (D) Yearly average IEPOX:$Sulf_{inorg}$ across the world for present-day conditions using the LMDz-OR-INCA global climate-chemistry model. White color indicates no sulfate (non-sea salt) or IEPOX concentration.

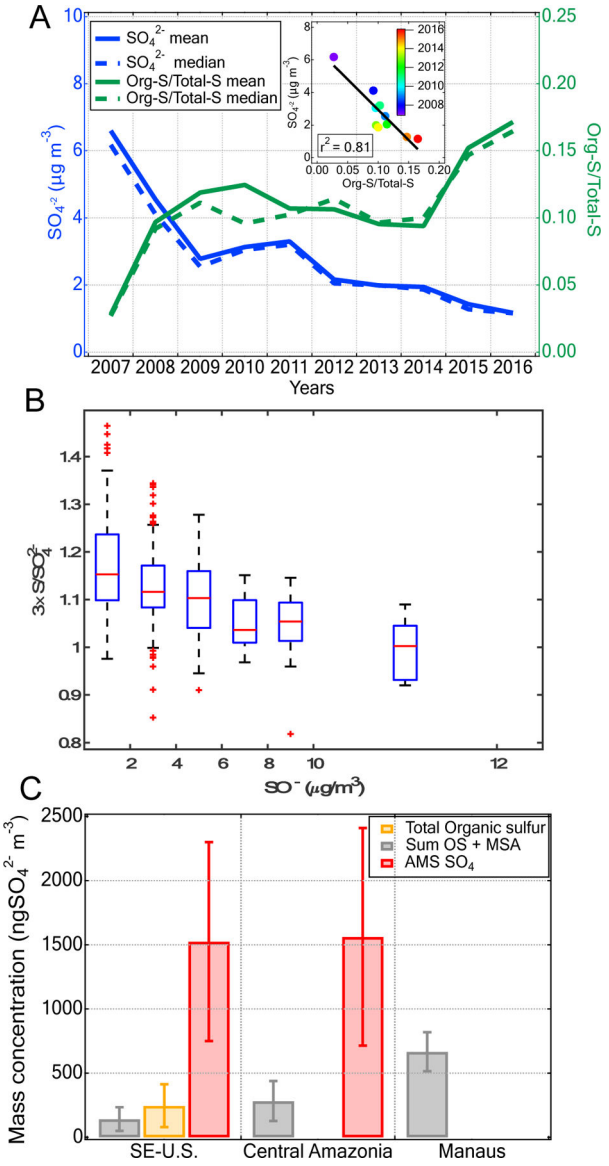

Figure 2.

(A) Correlation between total sulfate and organosulfur fraction and (B) Evolution of organosulfur fraction as a function of $Sulf_{inorg}$ at the Great Smoky Mountain Site (Look Rock, TN) during summer (May – September) from 2007–2016, using the National Park Service IMPROVE $PM_{2.5}$ database. If particulate organosulfur compounds are not present, the sulfate (SO_4^{2-}) mass measured by IC should equal three times the sulfur mass concentration measured by X-ray fluorescence (XRF), since the molar mass of sulfur and sulfate are 32 and 96 g/mol, respectively. A value of 3×S/ SO_4^{2-} lower than 1 is caused by the limitation of the analytical techniques to differentiate 3×sulfur from SO_4^{2-}.[42] (C) Average mass concentration of the identified organosulfates + methane sulfonic acid (OS + MSA) and total organosulfur compounds (Org-S) in the $PM_{2.5}$ samples collected during the 2013 SOAS campaign as well as the average mass concentrations of the sum of OS + MSA

quantified in downwind Manaus and Manaus. AMS data from SE-U.S. and downwind Manaus are also presented.

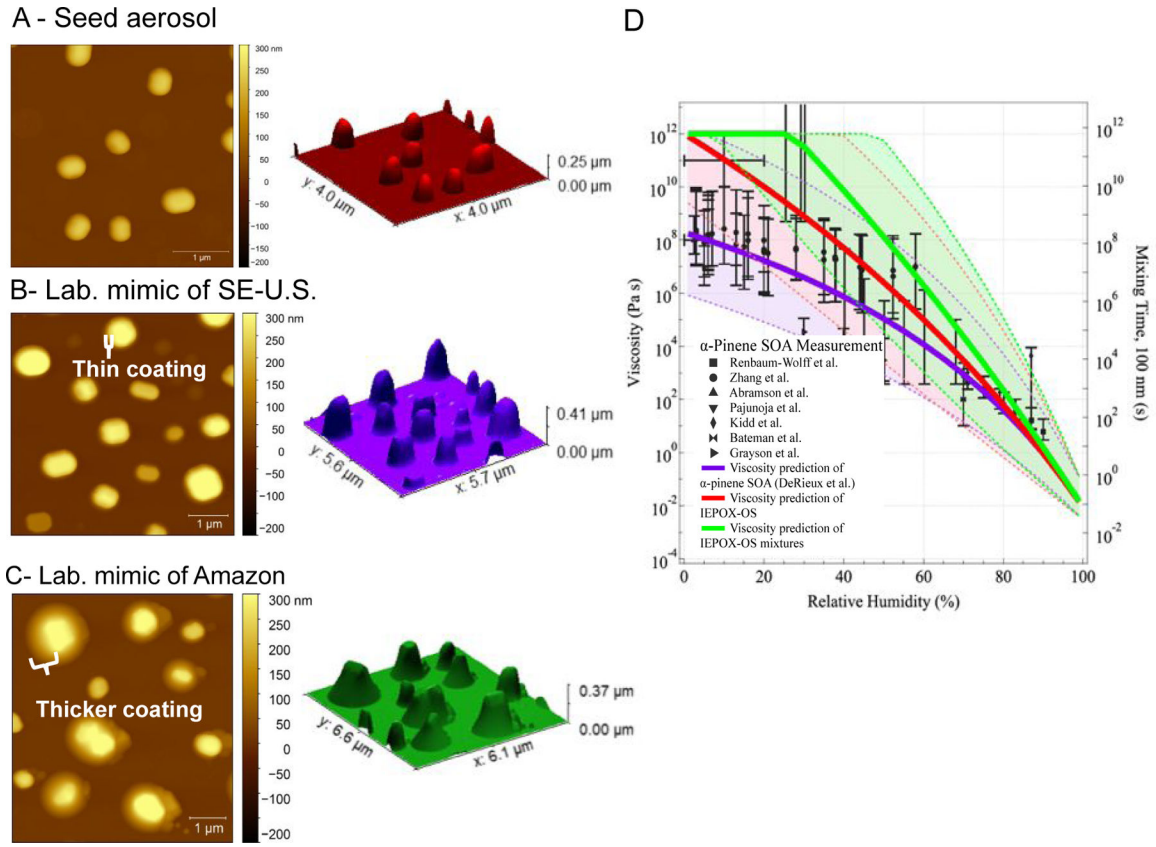

Figure 3.

Left Column (A), (B), and (C). Atomic force microscopy (AFM) height images of ammonium bisulfate seed (ABS), IEPOX-SOA generated from the reactive uptake of IEPOX in the presence of wet acidic aerosol at RH~50% and IEPOX:$Sulf_{inorg}$ ratios atmospherically relevant to laboratory mimic of SE-U.S. and Amazon, respectively. Middle column (A), (B), and (C). Height maps of impacted particles. (D) Comparison of the measured and predicted viscosity of α-pinene SOA (purple), predicted IEPOX-OS (red) and IEPOX-OS mixtures at 298 K as a function of RH. The data points represent measured viscosity values of α-pinene SOA. The solid lines represent estimated viscosity of α-pinene SOA,[66] IEPOX-OS, and IEPOX-OS mixtures (IEPOX-OS + Oligomeric-OS). The shaded areas represent the upper and lower bounds of the viscosity estimation for each type of SOA. Model parameters are: glass transition temperature of dry SOA ($T_{g,org}$); hygroscopicity (κ), fragility (D), and Gordon–Taylor constant (k_{GT}). Solid line for - pinene SOA at 278.5K: $T_{g,org}$ = 0.1, κ = 10, k_{GT} = 2.5. Solid line for 2-methyltetrol sulfate at 298K; $T_{g,org}$ = 0.12, κ = 13, k_{GT} = 2.5.; Solid line for IEPOX-derived OS mixture at 313 K, $T_{g,org}$ = 0.12, κ = 13, k_{GT} = 2.5. For upper (lower) bounds (shaded regions): α-pinene SOA; $T_{g,org}$ = 300 K (268.5 K), κ = 0.1 (0.1), D = 20 (10), k_{GT} = 2.5 (3.0). 2-Methyltetrol sulfate; $T_{g,org}$ = 320 K (288 K), κ = 0.10 (0.15), D = 20 (10), k_{GT} = 2.5 (3.0). OS mixture; $T_{g,org}$ = 330 K (303 K), κ = 0.10 (0.15), D = 20 (10), k_{GT} = 2.5 (3.0).

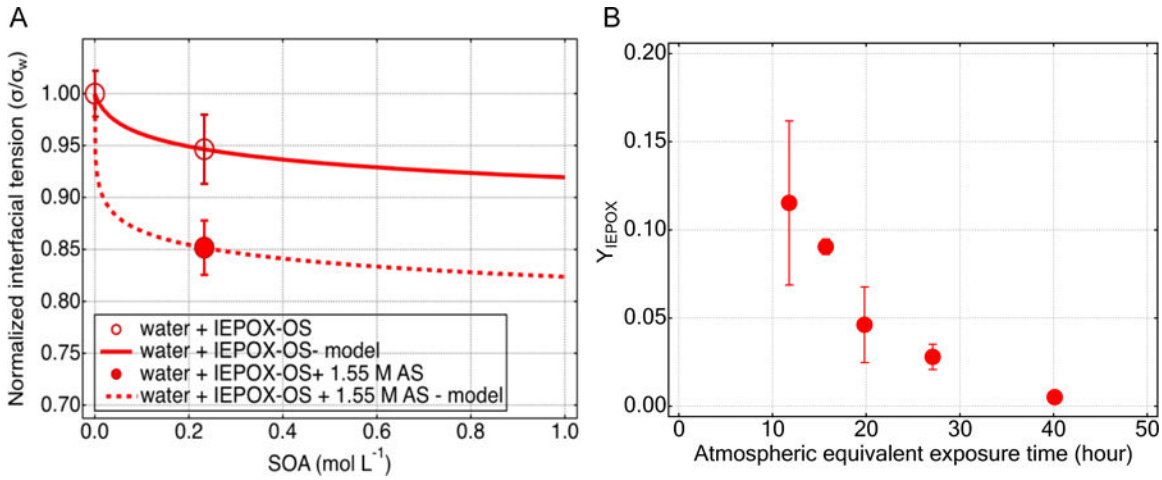

Figure 4.

(A) Measured and modeled interfacial tension (IFT) of IEPOX-OS. Microfluidic measurements of IFT (circles); two parameter model treatment of SOA in pure water (solid line), using a binary model [63,100] ; and model treatment of SOA in ammonium sulfate (AS) solution (dashed line), using an adapted form of the binary model adapted for salt-containing organic aqueous solutions that includes known organic model parameters from the solid line and the Setschenow constant as the single adjustable model parameter (dashed line). (B) IEPOX reactive uptake coefficient (γ_{IEPOX}), obtained from flow tube experiments performed at the University of Washington, on aqueous ammonium bisulfate particles as a function of atmospheric equivalent exposure time defined as the length of the time that an aerosol is exposed to IEPOX gases, assuming gas-phase IEPOX concentration of 1 ppb and an aerosol surface area density of 300 μm^2 cm^{-3}. The atmospheric equivalent exposure time is obtained from the experimental reaction time by multiplying the ratio of experimental-to-ambient concentration of IEPOX (=75) represents an upper limit.